Contents lists available at ScienceDirect

Engineering Structures

journal homepage: www.elsevier.com

Modified cracked membrane model for consistent crack width predictions of reinforced concrete structures subjected to in-plane loading

Reignard Tan [a, *], Max A.N. Hendriks [a, b], Mette Geiker [a], Terje Kanstad [a]

[a] Department of Structural Engineering, Norwegian University of Science and Technology, Trondheim, Norway
[b] Faculty of Civil Engineering & Geosciences, Delft University of Technology, Delft, the Netherlands

ARTICLE INFO

Keywords:
Crack widths
Crack spacing
Calculation model
RC membranes
In-plane loading
Tension stiffening
Modelling uncertainty

ABSTRACT

The modified cracked membrane model (MCMM) presented in this paper was formulated to facilitate a mechanical calculation model that predicts crack widths in reinforced concrete (RC) structures subjected to in-plane loading for all cracking stages. It was formulated using the basic concepts of the existing cracked membrane model (CMM). Furthermore, a generalized approach for predicting the tension stiffening normal to a crack was formulated, an approach currently lacking in Eurocode 2 and *fib* Model Code 2010. A simplified approach for predicting the cracking behaviour of RC membranes was also proposed. Comparison with a total of 101 maximum crack widths measured experimentally on 37 test specimen from the literature showed that the MCMM provided good and consistent crack width predictions even for the cases of large rebars and covers, at which the CMM was seen to struggle. The results in this paper suggests that both the MCMM and the simplified approach show great potential for yielding reliable crack width predictions in RC membranes.

Nomenclature

List of notations

A_c	sectional area
A_s	area rebar
c_b	center of Mohr's circle of concrete stresses between cracks
dx	differential element in an RC tie
E_c	Young's modulus concrete
E_p	Young's modulus prestressing steel
E_{ph}	Young's modulus prestressing steel after yielding
E_s	Young's modulus rebar
E_{sh}	Young's modulus rebar after yielding
f_{cm}	compressive strength concrete
f_{ct}	tensile strength concrete
f_{pu}	ultimate strength prestressing steel
f_{py}	yield strength prestressing steel
f_{su}	ultimate strength rebar
f_{sy}	yield strength rebar
G_f	tensile fracture energy concrete
k_c	reduction factor for compressive strength of concrete due to tensile strains
L	bar length
r_b	radius of Mohr's circle of concrete stresses between cracks
S_{cr}	crack spacing at biaxial stress conditions
S_{crx}	crack spacing in x-direction at biaxial stress conditions
S_{cry}	crack spacing in y-direction at biaxial stress conditions
S_{crx0}	maximum crack spacing in x-direction
S_{cry0}	maximum crack spacing in y-direction
S_{cr0}	crack spacing at uniaxial stress conditions
S_r	transfer length at biaxial stress conditions
S_{r0}	transfer length at uniaxial stress conditions
S_{rx0}	transfer length in x-direction
S_{ry0}	transfer length in y-direction
u	slip
$u_{r,CHLM}$	slip at the crack for CHLM
$u_{r,CLLM}$	slip at the crack for CLLM
u'	derivative of slip
w_{cr}	crack width predicted
$w_{cr,CMM}$	crack widths predicted by the cracked membrane model

* Corresponding author at: Multiconsult AS, Postboks 265 Skøyen, 0213 Oslo, Norway.
Email address: reignard.tan@multiconsult.no (R. Tan)

https://doi.org/10.1016/j.engstruct.2019.109362
Received 14 January 2019; Received in revised form 23 April 2019; Accepted 28 June 2019
Available online xxx
0141-0296/

$w_{cr,MCMM}$	crack widths predicted by the modified cracked membrane model
$w_{cr,simp}$	crack widths predicted by the simplified approach
w_{max}	crack width measured experimentally
x	coordinates in x-direction
y	coordinates in y-direction
ε_1	mean maximum principle strains
ε_c	concrete strains
ε_{c0}	concrete strains corresponding to the compressive strength of concrete
ε_{c1}	mean maximum principle strains in concrete
ε_{ct}	concrete strains corresponding to tensile strength of concrete
ε_{cx}	concrete strains in x-direction
ε_{cy}	concrete strains in y-direction
$\varepsilon_{c,max}$	maximum concrete strains
ε_{cm}	mean concrete strains
ε_{cmx}	mean concrete strains in x-direction
ε_{cmy}	mean concrete strains in y-direction
ε_m	mean strains
ε_p	prestressing steel strains
ε_{py}	prestressing steel strains at yielding
ε_{pu}	prestressing steel strains at ultimate strength
ε_s	rebar strains
ε_{sm}	mean rebar strains
ε_{smx}	mean rebar strains in x-direction
ε_{smy}	mean rebar strains in y-direction
ε_{sr}	rebar strains at the crack
$\varepsilon_{sr,y}$	rebar strains at the crack at yielding
ε_{sx}	rebar strains in x-direction
ε_{sy}	rebar strains in y-direction
$\varepsilon_{s,y}$	rebar strains at yielding
ε_{su}	rebar strains at ultimate strength
γ_{xy}	shear strains
γ_{cxy}	shear strains in concrete
ψ	factor accounting for plane sections not remaining plane in RC ties
ρ_{sx}	rebar ratio in x-direction
ρ_{sy}	rebar ratio in y-direction
σ_c	stresses in concrete
σ_{c1}	normal stresses in concrete normal to the crack
σ_{c1b}	maximum principle stresses in concrete between cracks
σ_{c2}	normal stresses in concrete parallel to the crack
σ_{cx}	normal stresses in concrete in x-direction
σ_{cy}	normal stresses in concrete in y-direction
σ_p	normal stresses in prestressing steel
σ_{prx}	normal stresses in prestressing steel at crack in x-direction
σ_{pry}	normal stresses in prestressing steel at crack in y-direction
σ_s	normal stresses in rebar in an RC tie
σ_{sr}	rebar stresses at crack
σ_{srx}	rebar stresses at crack in x-direction
σ_{sry}	rebar stresses at crack in y-direction
σ_x	normal stresses in x-direction
σ_y	normal stresses in y-direction
τ	bond stresses at the interface between concrete and steel
τ_{b0}	bond stresses at the interface between concrete and steel prior to yielding
τ_{b1}	bond stresses at the interface between concrete and steel after the onset of yielding
τ_{c12}	shear stresses in concrete at crack
$\tau_{m,y}$	bond stresses at the interface between concrete and steel at the onset of yielding of rebar at the crack
τ_{xy}	shear stresses
θ	modelling uncertainty
θ_{cr}	angle between a unit vector normal to the crack and x-direction
ϕ_s	rebar diameter

1. Introduction

There are many approaches for predicting crack widths in reinforced concrete (RC) structures exposed to uniaxial stress conditions and a comprehensive summary of them is provided in Borosnyói and Balász [7]. These calculation methods can be used to predict the cracking behaviour of one-way bearing structural elements such as RC ties, beams and slabs. However, they become inadequate for more complicated structural elements such as orthogonally RC membranes, two-way bearing slabs and shells. Such structural elements can in most practical cases be treated as components subjected to in-plane loading thus necessitating more comprehensive calculation methods, e.g. the modified compression field theory (MCFT) developed by Vecchio and Collins [64], Collins and Mitchell [11], Bentz [4] and Bentz et al. [5], the rotating angle softened-truss-model (RA-STM) developed by Hsu [30], Pang and Hsu [50], Hsu and Mo [31] and Bernardo et al. [6] and the cracked membrane model (CMM) developed by Kaufmann [37], Kaufmann and Marti [38], Foster and Marti [24], Dabbagh and Foster [12] and Pimentel et al. [51]. The three models have all proven to predict deformations and ultimate load capacity of structural elements subjected to in-plane loading, such as orthogonally RC membranes quite convincingly. Common for the models is that equilibrium of stresses is obtained iteratively in terms of the mean strains. The main differences between the models are that (i) equilibrium was formulated in terms of average stresses and average strains between cracks for the MCFT and the RA-STM, while equilibrium of stresses was formulated at the cracks for the CMM and (ii) tension stiffening was incorporated using empirical constitutive laws for the MCFT and the RA-STM, while tension stiffening was incorporated using the fully mechanical based tension chord model (TCM) developed by Marti et al. [44] for the CMM. Nonetheless, all three models could potentially predict crack widths under the presumption of assuming that a finite crack pattern had formed. In other words, the models can in principle predict crack widths in RC membranes for the *stabilized cracking stage* only.

The semi-empirical calculation methods for predicting crack widths recommended by Eurocode 2 (EC2) [8] and *fib* Model Code 2010 (MC2010) [26] were partially based on the same mechanical concept as the TCM [57]. However, EC2 and MC2010 do not provide complete guidelines for predicting cracking widths in RC membranes, i.e. they only offer a way of predicting the crack spacing but not the tension stiffening normal to the crack. There have been some proposals for this in the literature, though without avoiding incorporating tension stiffening in an empirical manner [9,27]. Using empirical constitutive laws for the tension stiffening can limit the models' range of applicability as it in general depends on the bond behaviour between concrete and steel, and is further governed mechanically by the cover, diameter of the reinforcing steel bars (rebars), rebar spacing and load level [41,28,47,17,46,56,34,61,58]. Further comparing the comprehensive calculation methods shows that the CMM offers the possibility of altering the basic components that govern its mechanical behaviour quite conveniently. It can thus be argued that the CMM offers greater potential in predicting the cracking behaviour of RC membranes subjected to in-plane loading than the MCFT and RA-STM. A statement also acknowledged by the state-of-the-art French research project CEOS.fr [2].

This study is part of an ongoing research project with the overall objective of improving crack width calculation methods for large-scale concrete structures planned for the coastal high-way route "Ferry-free E39" in Norway. Use of large covers being up to 130 mm is specified by the Norwegian Public Roads Administration (NPRA) guidelines N400 [48] for marine structures. In addition, large rebar diameters, often in bundles and over several layers, are typically used for the cross-sections of such large-scale concrete structures. It was shown by Tan et al. [57] that Eurocode 2 with German National Annex [16], which essentially is similar to the TCM, predicted maximum crack widths inconsistently and in average on the nonconservative side particularly for the combination of large rebars and covers. This led to formulating the *modified tension chord model* (MTCM), which has proven to predict the cracking behaviour of RC ties more consistently and on the conservative side regardless of cover and rebar size [60]. In this paper, the CMM is used to formulate a new calculation model for predicting the response of orthogonally RC membranes, later referred to as the *modified cracked membrane model* (MCMM). In shortness, the MCMM incorporates tension stiffening using the MTCM instead of the TCM to account for the cracking behaviour in the *crack formation stage* and the stabilized cracking stage, as well as after yielding of reinforcement. Tan et al. [58] showed that the crack formation stage could be governing even at relatively large steel stresses in cases with large covers.

First, the basic principles in the CMM are discussed after which the MTCM is derived and incorporated in the MCMM together with a set of chosen constitutive models for concrete, reinforcing steel and prestressing steel. Based on the MCMM, a simplified approach for predicting crack widths in RC membranes is proposed. Then, crack widths predicted by the MCMM, CMM and the simplified approach are compared to a total of 101 maximum crack widths measured from experiments on 37 test specimen reported in the literature. Finally, the modelling uncertainty for the three models is discussed.

2. Cracked membrane model

2.1. The basic principles

The equilibrium equations of stresses at cracks can be obtained by e.g. orienting the unit vectors $\boldsymbol{n}$ and $\boldsymbol{e}$ in the direction of the inflicted stresses σ_x, σ_y and τ_{xy} [32] as shown in Fig. 1

$$\sigma_x = \sigma_{c1}\cos^2\theta_{cr} + \sigma_{c2}\sin^2\theta_{cr} - 2\tau_{c12}\sin\theta_{cr}\cos\theta_{cr} + \rho_{sx}\sigma_{srx} + \rho_{px}\sigma_{prx} \quad (1)$$

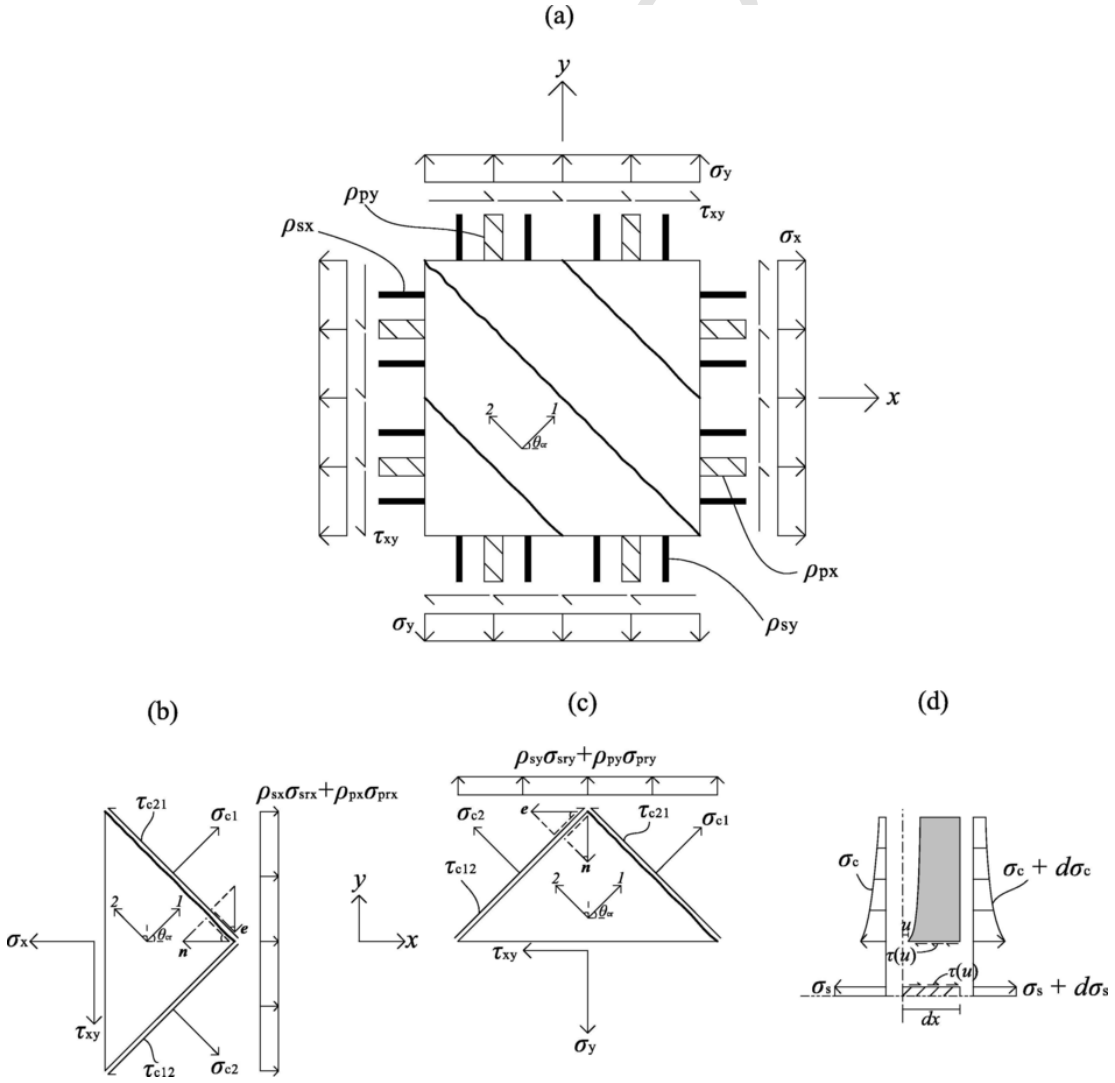

Fig. 1. (a) Cracked RC membrane. (b) and (c) Equilibrium of stresses at the crack in x- and y-direction. (d) Stresses, deformations and slip for a differential element in an RC tie.

$$\sigma_y = \sigma_{c1}\sin^2\theta_{cr} + \sigma_{c2}\cos^2\theta_{cr} + 2\tau_{c12}\sin\theta_{cr}\cos\theta_{cr} + \rho_{sy}\sigma_{sry} + \rho_{py}\sigma_{pry} \quad (2)$$

$$\tau_{xy} = (\sigma_{c1} - \sigma_{c2})\sin\theta_{cr}\cos\theta_{cr} + \tau_{c12}\left(\cos^2\theta_{cr} - \sin^2\theta_{cr}\right) \quad (3)$$

where σ_{c1} are concrete stresses normal to the crack, σ_{c2} are concrete stresses parallel to the crack, τ_{c12} are shear stresses at the crack, σ_{srx} and σ_{sry} are rebar stresses at the crack in x and y-direction respectively, ρ_{sx} and ρ_{sy} are steel reinforcement ratios in x and y-direction respectively, σ_{prx} and σ_{pry} are prestressing steel stresses at the crack in x and y-direction respectively, ρ_{px} and ρ_{py} are prestressing steel ratios in x and y-direction respectively and θ_{cr} is the angle between a unit vector normal to the crack and the global x-direction. The cracks are assumed free to rotate implying null shear stresses at cracks, i.e. $\tau_{c12} = 0$, and that the cracked plane is coincident with the plane of principal strains. Internal stresses in Eqs. (1)–(3) are finally obtained through a set of chosen constitutive models for concrete, steel and tension stiffening in terms of the global mean strains ε_x, ε_y and γ_{xy}.

2.2. Tension chord model

The second order differential equation (SODE) for the slip u was derived by considering equilibrium, compatibility and linear elastic material laws for steel and concrete for a differential element in an RC tie, see Fig. 1(d), or e.g. as discussed by Saliger [54], Russo and Romano [53], Balász [1], Khalfallah [35], *fib* bulletin No. 52 [25] and Debernardi and Taliano [15]

$$\frac{d^2u}{dx^2} - \chi\tau(u) = 0 \quad (4)$$

where τ was the bond stress at interface between concrete and steel, while $\chi = \frac{\sum\pi\phi_s}{A_sE_s}(1+\xi)$ was a constant with ϕ_s, A_s and E_s being the diameter, area and the Young's modulus respectively for the rebar. Furthermore, the other constants were defined as $\xi = \alpha_E\rho_s/\psi$, $\alpha_E = E_s/E_c$ and $\rho_s = A_s/A_c$, with A_c being the sectional area of the RC tie and E_c the Young's modulus for concrete, while $\psi \le 1.0$ was a factor accounting for that plane sections do not remain plane in RC ties [19]. Basically, $\psi \neq 1.0$ modifies the equilibrium equations for concrete and accounts for the fact that the strain profile over the cover is not constant in RC ties [59]. In general, Eq. (4) has to be solved using a bond-slip law $\tau(u)$ often necessitating numerical integration techniques, e.g. as proposed by, [1,15]. As a simplification, Marti et al. [44] developed the TCM, which was based on solving Eq. (4) for the stabilized cracking stage using a simple stepped, rigid-perfectly plastic bond-slip law where $\tau(u) = \tau_{b0} = 2f_{ct}$ for steel stresses prior to yielding and $\tau(u) = \tau_{b1} = f_{ct}$ after the onset of yielding with $\psi = 1.0$ thus assuming a constant strain profile over the cover. The CMM was formulated using the TCM to determine steel stresses at the cracks in terms of the mean strains [37,38]. The problem was that the response could not be predicted for lower steel stresses typically occurring at the crack formation stage. Seelhofer [55] partially solved this issue by including a formulation in the TCM that accounted for the behaviour at lower steel stresses, however, still under the assumption that a fixed crack pattern had formed.

3. Modified cracked membrane model

3.1. Modified tension chord model

3.1.1. General

The modified tension chord model (MTCM) is a tension stiffening model based on solving the SODE for the slip in Eq. (4) completely analytically using the bond-slip law of Eligehausen et al. [20] and later adopted by MC2010

$$\tau(u) = \tau_{max}\left(\frac{u}{u_1}\right)^{\alpha} \quad (5)$$

Here, $u_1 = 0.1$ mm, $\tau_{max} = 5.0$ MPa and $\alpha = 0.35$ being the chosen bond-slip parameters to account for the behaviour of RC ties according to the recommendations in Tan et al. [58]. The conceptual difference between the TCM and MTCM is visualized in Fig. 2(a) for steel stresses prior to yielding, in which the continuous and dashed lines represent steel strains ε_s and the corresponding concrete strains ε_c respectively. The linear curves show that the strains vary over the bar length with a constant slope of $4\tau_{b0}/\phi_s$ for the TCM, while nonlinear strains in general are observed for the MTCM. Furthermore, the tension stiffening can be subdivided into three regimes depending on if the steel stresses over the bar length are; (1) below yielding, (2) partially below and above yielding or (3) above yielding as pointed out by Kaufmann [37] and Kaufmann and Marti [38], see Fig. 2(b). An output from the MTCM is usually the mean steel strains ε_{sm} as a function of the steel stresses σ_{sr} at the crack similar to the concept of any other tension stiffening model, e.g. EC2, MC2010 or the TCM. The challenge, however, is to "go the other way around" and determine the steel stresses at the crack σ_{sr} as a function of mean strains ε_{sm} instead. For solving this inverse problem for Regime 1, the analytical solutions to the SODE for the slip fully provided in Russo and Romano [53] and Tan et al. [60] are used. For Regime 2 and 3, the closed form solutions provided by Kaufmann [37] and Kaufmann and Marti [38] are used, however, with modifications for the stepped, rigid-perfectly plastic bond-slip law to avoid abrupt change in stiffness between Regime 1 and 2. Moreover, the factor $\psi = 0.70$ was for the MTCM adopted according to the recommendations in Tan et al. [59], which was seen to remain constant and equal to this value except for a region close to the loaded end, regardless of the cover size, rebar diameter, load level and even material properties in the case of axisymmetry.

3.1.2. Regime 1

The response in Regime 1 is grouped into two concepts as *comparatively lightly loaded members* (CLLM) and *comparatively heavily loaded members* (CHLM), which in principle are analogous to the crack formation stage and the stabilized cracking stage respectively. The concept of CLLM is depicted in Fig. 3(a) and (b) in which the transfer length S_{r0} denotes the abscissa where steel and concrete strains become compatible and the slip becomes zero. It moves towards the symmetry section $L/2$ upon increasing the load and a new crack is formed at the location where the concrete strains exceed the tensile strength of concrete, i.e. $S_{r0} = S_{cr0}$ if $\varepsilon_c(S_{r0}) = \varepsilon_{c,max} \ge \varepsilon_{ct}$. Here, $\varepsilon_{ct} = f_{ct}/E_c$, f_{ct} being the tensile strength of concrete, while S_{cr0} is the crack spacing. The concept of CHLM governs thereafter the response for the newly cracked member in which it is observed that steel and concrete strains remain incompatible over the entire crack spacing although the slip is zero at the symmetry section as depicted in Fig. 3(c) and (d). In summary, the main difference between the two concepts is that strains become compatible at a certain location over the bar length for CLLM, while strains remain incompatible over the entire bar length for CHLM. This provided two sets of boundary conditions yielding closed form solutions for CLLM

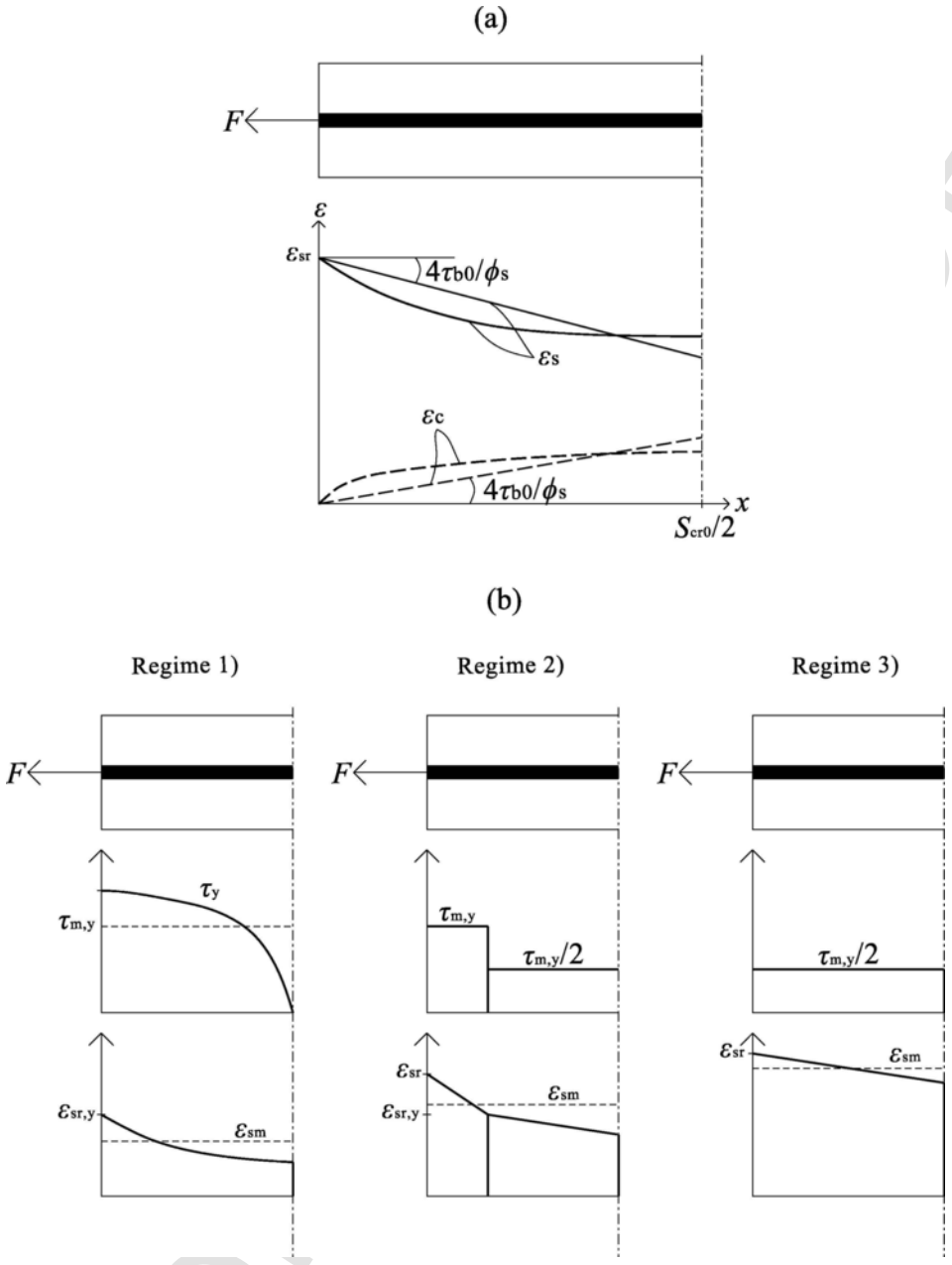

Fig. 2. (a) Steel and concrete strains distribution over the bar length. Linear strains represent the concept of TCM, while nonlinear strains represent the concept of MTCM. (b) Regime 1 represents steel stresses over the bar length prior to yielding. Regime 2 represents steel stresses over the bar length that partially are below and above yielding. Regime 3 represents steel stresses over the entire bar length that are above yielding.

and non-closed form solutions for CHLM. General expressions for the steel strains and concrete strains independent of the concept were obtained as

$$\varepsilon_s = \frac{\xi\varepsilon_{sr} - u'}{1+\xi} \tag{6}$$

$$\varepsilon_c = \psi\xi\frac{\varepsilon_{sr} + u'}{1+\xi} \tag{7}$$

in which $-u' = \varepsilon_s - \varepsilon_c$ was the derivative of the slip and $\varepsilon_{sr} = \sigma_{sr}/E_s$ was the steel strain at the crack. The expressions for mean steel strains and mean concrete strains are for CLLM obtained by integrating Eqs. (6) and (7) respectively over the transfer length S_{r0}

$$\varepsilon_{sm} = \frac{1}{S_{r0}}\frac{\xi\varepsilon_{sr}S_{r0} + u_{r,CLLM}}{1+\xi} \tag{8}$$

$$\varepsilon_{cm} = \frac{\psi\xi}{S_{r0}}\frac{\varepsilon_{sr}S_{r0} - u_{r,CLLM}}{1+\xi} \tag{9}$$

in which the transfer length was defined as

$$S_{r0} = \frac{1}{\delta}\left[\varepsilon_{sr}\left(\frac{1}{2\gamma}\right)^{\frac{1}{2\delta}}\right]^{\frac{2\delta}{\beta}} \tag{10}$$

while the slip at the crack was obtained as, see Fig. 3(b)

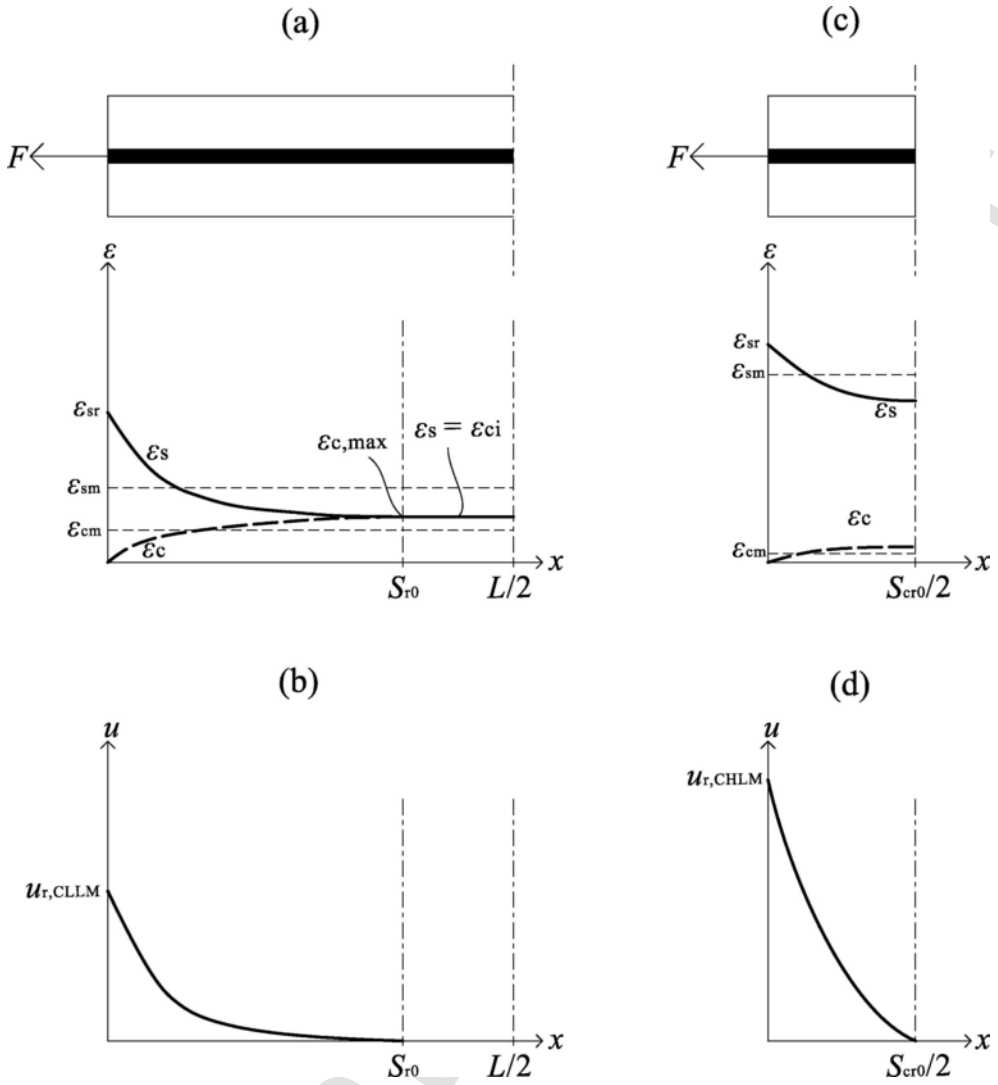

Fig. 3. (a) Steel and concrete strains distribution over the bar length for the concept of CLLM. (b) Slip over the bar length for the concept of CLLM. (c) Steel and concrete strains distribution over the bar length for the concept of CHLM. (d) Slip over the bar length for the concept of CHLM.

$$u_{\mathrm{r,CLLM}} = \left(\frac{1}{2\gamma}\right)^{\frac{1}{\beta}} \varepsilon_{\mathrm{sr}}^{\frac{2}{\beta}} \tag{11}$$

with the constants $\gamma = \chi\tau_{\max}/(\beta u_1^{\alpha})$, $\beta = 1+\alpha$ and $\delta = (1-\alpha)/2$. Inserting Eqs. (10) and (11) in (8), substituting $\varepsilon_{\mathrm{sm}}$ with a known value for the mean strains ε_{m} and multiplying with the Young's modulus for steel yields an expression for the steel stresses at the crack as

$$\sigma_{\mathrm{sr}} = \frac{1+\xi}{\delta+\xi}\varepsilon_{\mathrm{m}}E_{\mathrm{s}} \tag{12}$$

An expression for the steel stresses at the crack as a function of the mean strains is derived conveniently due to the closed form solution of the slip at the crack provided for CLLM. This is not the case for CHLM since the slip at the crack $u_{\mathrm{r,CHLM}}$ only could be obtained iteratively as a function of $\varepsilon_{\mathrm{sr}}$. Thus, a solution to obtain $\varepsilon_{\mathrm{sr}}$ for CHLM for a known value of the mean strain ε_{m} is by assuming

$$\varepsilon_{\mathrm{sr}} = \frac{\varepsilon_{\mathrm{m}}}{\beta_{\mathrm{s}}} \tag{13}$$

where $\beta_{\mathrm{s}} = 1$ is chosen initially. The expressions for mean steel strains and mean concrete strains are obtained in a similar fashion as for CLLM, however, this time around by integrating Eqs. (6) and (7) over half the crack spacing $S_{\mathrm{cr0}}/2$ according to Fig. 3(c)

$$\varepsilon_{\mathrm{sm}} = \frac{1}{\frac{S_{\mathrm{cr0}}}{2}} \frac{\xi\varepsilon_{\mathrm{sr}}\frac{S_{\mathrm{cr0}}}{2} + u_{\mathrm{r,CHLM}}}{1+\xi} \tag{14}$$

$$\varepsilon_{\mathrm{cm}} = \frac{\psi\xi}{\frac{S_{\mathrm{cr0}}}{2}} \frac{\varepsilon_{\mathrm{sr}}\frac{S_{\mathrm{cr0}}}{2} - u_{\mathrm{r,CHLM}}}{1+\xi} \tag{15}$$

in which the theoretical maximum crack spacing was defined as

$$S_{\mathrm{cr0}} = \frac{1}{\delta}\left[\varepsilon_{\mathrm{ct}}\frac{1+\xi}{\psi\xi}\left(\frac{1}{2\gamma}\right)^{\frac{1}{2\delta}}\right]^{\frac{2\delta}{\beta}} \tag{16}$$

The maximum slip $u_{\mathrm{r,CHLM}}$ is determined iteratively as a function of $\varepsilon_{\mathrm{sr}}$ using the solution strategy provided in [60]. If $\varepsilon_{\mathrm{sm}} \neq \varepsilon_{\mathrm{m}}$, new values of $\beta_{\mathrm{s}} = \varepsilon_{\mathrm{sm}}/\varepsilon_{\mathrm{sr}} \leq 1$, $\varepsilon_{\mathrm{sr}}$ using Eq. (13) and $\varepsilon_{\mathrm{sm}}$ using Eq. (14) are calculated. Finally, steel stresses at the crack are obtained by multiplication

of Eq. (13) with the Young's modulus for steel

$$\sigma_{sr} = \frac{\epsilon_m}{\beta_s} E_s \tag{17}$$

3.1.3. Regime 2 and 3

Regime 2 and 3, which represent steel stresses over the crack spacing after the onset of yielding, is in general not relevant in terms of serviceability but are needed to properly account for cases where the reinforcement ratio in one direction differs greatly from the other direction. This could cause yielding for the reinforcement with lowest reinforcement ratio while the other remains elastic. The expressions for the steel stresses provided in the TCM [37,38] are used as a simplification. However, one important modification in relation to the stepped, rigid-perfectly plastic bond-slip law is applied. Instead of directly relating the mean bond stresses to the tensile strength of concrete as $\tau(u) = \tau_{b0} = 2f_{ct}$ and $\tau(u) = \tau_{b1} = f_{ct}$, they are rather taken as the mean bond stress $\tau_{m,y}$ of the bond stress distribution τ_y at the onset of yielding of the rebar at the crack, i.e. when $\epsilon_{sr} = \epsilon_{sr,y} = f_{sy}/E_s$ where f_{sy} is the yield stress. This means that $\tau(u) = \tau_{m,y}$ for steel stresses prior to yielding and $\tau(u) = \tau_{m,y}/2$ for steel stresses after the onset of yielding, see Fig. 2(b). This is mainly to avoid abrupt change in stiffness in the transition between Regime 1 and 2. The expression for Regime 2 becomes

$$\sigma_{sr} = f_{sy} + 2\frac{\frac{\tau_{m,y}S_{cr0}}{\phi_s} - \sqrt{\left(f_{sy} - E_s\epsilon_m\right)\frac{\tau_{m,y}S_{cr0}}{2\phi_s}\left(2 - \frac{E_s}{E_{sh}}\right) + \frac{E_s}{E_{sh}}\frac{\tau_{m,y}^2}{2}\frac{S_{cr0}^2}{\phi_s^2}}}{2 - \frac{E_s}{E_{sh}}} \tag{18}$$

for $\frac{f_{sy}}{E_s} - \frac{\tau_{m,y}S_{cr0}}{\phi_s E_s} < \epsilon_m \le \frac{f_{sy}}{E_s} + \frac{\tau_{m,y}S_{cr0}}{2\phi_s E_{sh}}$, while the expression for Regime 3 becomes

$$\sigma_{sr} = f_{sy} + \left(\epsilon_m - \frac{f_{sy}}{E_s}\right)E_{sh} + \frac{\tau_{m,y}S_{cr0}}{2\phi_s} \tag{19}$$

for $\epsilon_m > \frac{f_{sy}}{E_s} + \frac{\tau_{m,y}S_{cr0}}{2\phi_s E_{sh}}$.

3.1.4. Constitutive model

The stress-strain curves for the constitutive models of MTCM, TCM and naked steel are plotted in Fig. 4 with two different reinforcement configurations. Fig. 4(a) applied to an RC tie with $\rho_s = 2.93\%$, $\phi_s = 19.5$ mm, $f_{sy} = 492$ MPa and $\tau_{m,y} = 4.196$ MPa, while Fig. 4(b) applied to an RC tie with $\rho_s = 0.97\%$, $\phi_s = 11.3$ mm, $f_{sy} = 479$ MPa and $\tau_{m,y} = 4.673$ MPa. The Young's modulus for steel was set to $E_s = 200000$MPa, while the cylinder strength, tensile strength and the Young's modulus for concrete was set to $f_c = 42.5$ MPa, $f_{ct} = 3.17$ MPa and $E_c \approx 34,000$ MPa respectively in both cases. The bar length was set equal to the crack spacing determined by the MTCM and TCM as 265 mm and 161 mm respectively in Fig. 4(a) and as 286 mm and 311 mm respectively in Fig. 4(b). It is observed that the TCM is slightly stiffer in its response than the MTCM. Furthermore, it is noticed a drop of steel stresses for the MTCM at $\epsilon_m \approx 1{\cdot}10^{-3}$ in Fig. 4(a), which can be explained by the fact that the CHLM behaviour allows for a crack to form at the centre of the crack spacing if the concrete strains at this location exceed the tensile strength of concrete, i.e. when $\epsilon_c(S_{cr0}/2) \ge \epsilon_{ct}$, as recommended by Russo and Romano [53] and Tan et al. [60].

3.2. Modified tension chord model at biaxial stress conditions

3.2.1. General

The MTCM at biaxial stress conditions caused by in-plane loading is discussed by considering the development of maximum principle stresses of concrete between cracks. The consideration of Mohr's circle of concrete stresses at cracks and between cracks depicted in Fig. 5 yields an expression for the development of maximum principle stresses in the concrete as

$$\sigma_{c1b} = \frac{f_{ct}}{2}\left(\lambda_x + \lambda_y\right) - \frac{\tau_{xy}}{2}\left(\tan\theta_{cr} + \cot\theta_{cr}\right) + \sqrt{\left[\frac{\tau_{xy}}{2}\left(\cot\theta_{cr} - \tan\theta_{cr}\right)\right]^2 - \frac{f_{ct}}{2}\left(\lambda_x - \lambda_y\right) + \tau_{xy}^2} \le f_{ct} \tag{20}$$

under the assumption that θ_{cr} and τ_{xy} remain the same, where $\lambda_x = \epsilon_{cx,max}/\epsilon_{ct}$ and $\lambda_y = \epsilon_{cy,max}/\epsilon_{ct}$. In general,

$$\lambda = \frac{\epsilon_{c,max}}{\epsilon_{ct}} \le 1 \tag{21}$$

where $\epsilon_{c,max}$ are maximum concrete strains at the end of the transfer length S_{r0}, see Fig. 3(a), in which the expression according to Russo and Romano [53] and Tan et al. [60] is adopted

$$\epsilon_{c,max} = \frac{\psi\xi}{1+\xi}\epsilon_{sr} \tag{22}$$

Here, ϵ_{sr} is determined from Eq. (12) implying that λ becomes a value dependent on the steel stresses at the crack. The limiting value in Eq. (21) is chosen such that the transfer length S_{r0} never is larger than the crack spacing S_{cr0} in the uniaxial direction. Furthermore, it can be proven that the limit state in Eq. (20), i.e. when $\sigma_{c1b} = f_{ct}$, only is attained for $\lambda_x = \lambda_y = 1$. This also means that the cracking response in biaxial stress conditions is determined either by the concept of CLLM or CHLM similar to uniaxial stress conditions as depicted in Fig. 6.

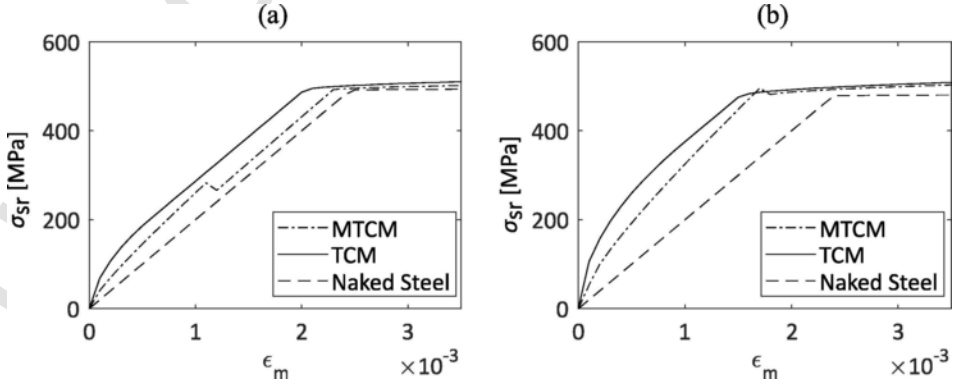

Fig. 4. (a) Stress strain curve for an RC tie with $\rho_s = 2.93\%$, $\phi_s = 19.5$ mm, $f_{sy} = 492$ MPa and $\tau_{m,y} = 4.196$ MPa. Bar lengths are set to 265 mm and 161 mm for the MTCM and the TCM respectively. (b) Stress strain curve for an RC tie with $\rho_s = 0.97\%$, $\phi_s = 11.3$ mm, $f_{sy} = 479$ MPa and $\tau_{m,y} = 4.673$ MPa. Bar lengths are set to 286 mm and 311 mm for the MTCM and TCM.

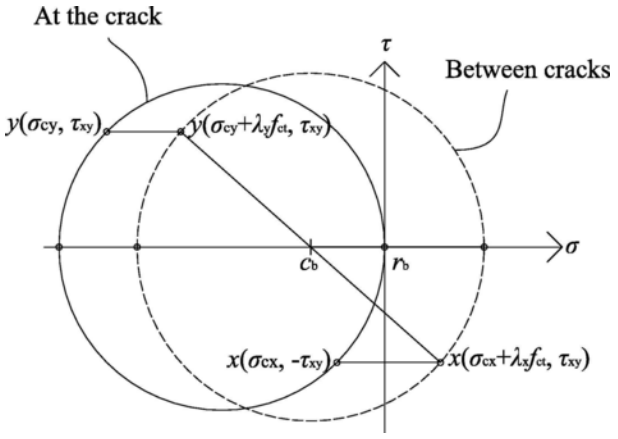

Fig. 5. Figure of Mohr's circle of stresses for the concrete at cracks and between cracks inspired by Kaufmann and Marti [38].

3.2.2. CLLM

The concept of CLLM at biaxial stress conditions implies that $\lambda_x < 1$, $\lambda_y < 1$ and $\sigma_{c1b} < f_{ctm}$, meaning only a distinct region $S_r/2$ to each side of the crack experiences incompatibility in strains, see Fig. 6(a). By geometry, two conditions for the transfer length apply

$$S_r = \begin{cases} 2S_{rx0}\cos|\theta_{cr}| \text{ if} S_{rx0}\cos|\theta_{cr}| \geq S_{ry0}\sin|\theta_{cr}| \\ 2S_{ry0}\sin|\theta_{cr}| \text{ if} S_{rx0}\cos|\theta_{cr}| < S_{ry0}\sin|\theta_{cr}| \end{cases} \quad (23)$$

in which S_{rx0} and S_{ry0} are determined from Eq. (10), while steel stresses at the crack are determined using Eq. (12).

3.2.3. CHLM

It is assumed that the concept of CHLM governs as long as either $\lambda_x = 1$, $\lambda_y = 1$ or $\sigma_{c1b} = f_{ct}$ occur. The choice means that the reinforcement in one direction can be governed by CLLM behaviour ($\lambda < 1$), while the other can be governed by CHLM behaviour ($\lambda = 1$), which typically occur in cases with orthotropic reinforcement configurations and for load situations with low shear stresses compared to the normal stresses. This means that CHLM governs as long as one of the reinforcement directions is governed by CHLM behaviour. Fig. 6(b) shows the case when $\lambda_x = 1$, $\lambda_y = 1$ and $\sigma_{c1b} = f_{ct}$ occur simultaneously. By geometry and the fact that the limit state, i.e. $\sigma_{c1b} = f_{ctm}$, only is attained for $\lambda_x = 1$ and $\lambda_y = 1$ yields two conditions for the crack spacing that is chosen to apply

$$\left.\begin{array}{c} S_{crx} = S_{crx0} \\ S_{cr} = S_{crx}\cos|\theta_{cr}| \\ S_{cry} = \dfrac{S_{cr}}{\sin|\theta_{cr}|} \end{array}\right\} \text{ if } S_{crx0}\cos|\theta_{cr}| \geq S_{cry0}\sin|\theta_{cr}| \quad (24)$$

or as

$$\left.\begin{array}{c} S_{cry} = S_{cry0} \\ S_{cr} = S_{cry}\sin|\theta_{cr}| \\ S_{crx} = \dfrac{S_{cr}}{\cos|\theta_{cr}|} \end{array}\right\} \text{ if } S_{crx0}\cos|\theta_{cr}| < S_{cry0}\sin|\theta_{cr}| \quad (25)$$

meaning that the skew crack spacing simply is governed by the angle θ_{cr} and the theoretical maximum crack spacing in uniaxial directions determined from Eq. (16). Fig. 6 shows the case where $S_{rx0}\cos|\theta| > S_{ry0}\sin|\theta|$ and $S_{crx0}\cos|\theta| > S_{cry0}\sin|\theta|$, in which it is noticed that line *AB* in Fig. 6(a) later forms to a crack in Fig. 6(b). Steel stresses at the crack are determined in a similar fashion as discussed for Eq. (17), however, by substituting the crack spacing S_{cr0} in Eq. (14) with S_{crx} and S_{cry}. Similar substitution applies for Eqs. (18) and (19) in Regime 2 and 3.

3.2.4. Crack width

The crack width is for the concept of CLLM determined as

$$w_{cr} = S_r(\varepsilon_1 - \varepsilon_{c1}) \quad (26)$$

and for the concept of CHLM as

$$w_{cr} = S_{cr}(\varepsilon_1 - \varepsilon_{c1}) \quad (27)$$

where ε_1 and ε_{c1} are mean maximum principle strains for the RC membrane and the concrete respectively determined as

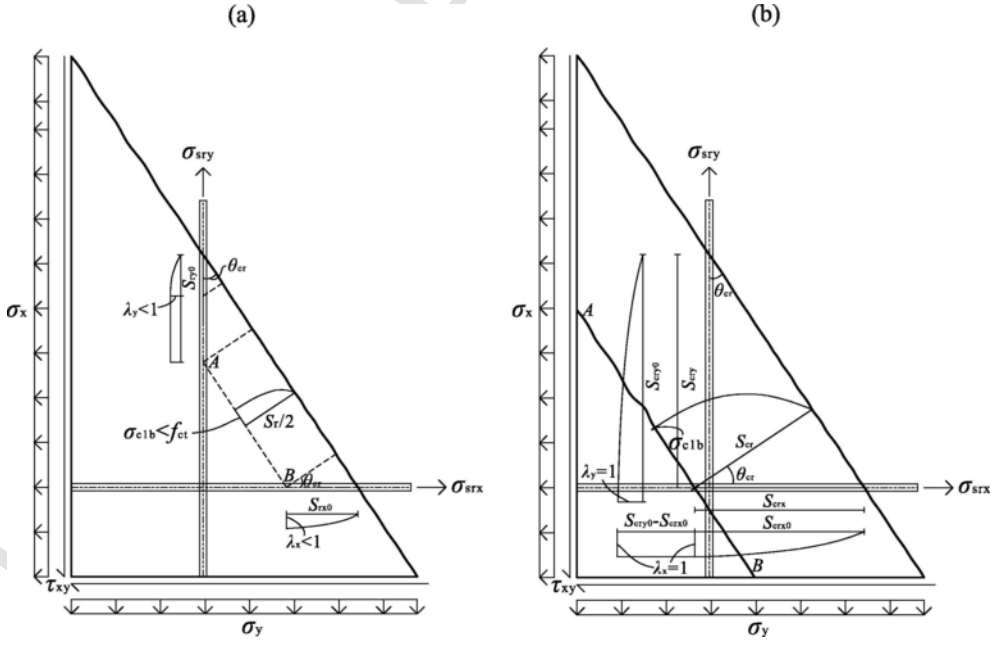

Fig. 6. (a) CLLM at biaxial stress conditions. (b) The limit state and CHLM at biaxial stress conditions.

$$\varepsilon_1 = \frac{\varepsilon_{smx} + \varepsilon_{smy}}{2} + \sqrt{\left(\frac{\varepsilon_{smx} - \varepsilon_{smy}}{2}\right)^2 + \left(\frac{\gamma_{xy}}{2}\right)^2} \tag{28}$$

$$\varepsilon_{c1} = \frac{\varepsilon_{cmx} + \varepsilon_{cmy}}{2} + \sqrt{\left(\frac{\varepsilon_{cmx} - \varepsilon_{cmy}}{2}\right)^2 + \left(\frac{\gamma_{cxy}}{2}\right)^2} \tag{29}$$

Conservatively neglecting the concrete shear strains γ_{cxy} and subtracting Eq. (29) from (28) yields

$$\varepsilon_1 - \varepsilon_{c1} = \frac{(\varepsilon_{smx} - \varepsilon_{cmx}) + (\varepsilon_{smy} - \varepsilon_{cmy})}{2} + \sqrt{\left(\frac{\varepsilon_{smx} - \varepsilon_{smy}}{2}\right)^2 + \left(\frac{\gamma_{xy}}{2}\right)^2} - \left|\frac{\varepsilon_{cmx} - \varepsilon_{cmy}}{2}\right| \tag{30}$$

which is approximately the same as

$$\varepsilon_1 - \varepsilon_{c1} \approx \frac{(\varepsilon_{smx} - \varepsilon_{cmx}) + (\varepsilon_{smy} - \varepsilon_{cmy})}{2} + \sqrt{\left[\frac{(\varepsilon_{smx} - \varepsilon_{cmx}) - (\varepsilon_{smy} - \varepsilon_{cmy})}{2}\right]^2 + \left(\frac{\gamma_{xy}}{2}\right)^2} \tag{31}$$

The expression in Eq. (31) was formulated with the purpose of serving as a generalized approach for predicting tension stiffening in skew cracks, an expression currently lacking in EC2 and MC2010. The expression is thus dependent on (i) the difference between the mean strains, $\varepsilon_{sm} - \varepsilon_{cm}$, making it compatible with any other tension stiffening model for uniaxial stress conditions and (ii) the shear strains γ_{xy} known from equilibrium.

3.3. Steel

Bilinear material behaviour is assumed for both reinforcing steel and prestressing steel as shown in Fig. 7.

3.4. Concrete

The constitutive model elaborated in Foster and Marti [24] is here adopted for the compressive behaviour of concrete, see Fig. 8(a). Briefly summarized, the compressive curve by Thorenfeldt et al. [62] was adopted using the calibrated decay factor proposed by Collins and Porasz [10] for the post peak behaviour of conventional and high strength concrete. Furthermore, the stress and strain peak was adjusted by the factor k_c, which was obtained using the model of Vecchio and Collins [64] to account for weakening of concrete when subjected to biaxial tension compression, i.e. $k_c \leq 1$. The effect of confinement, i.e. when $k_c > 1$, is by the authors of this paper conservatively neglected.

Tension softening is in general neglected, except for the condition when both principle strains are positive, i.e. $\varepsilon_1 \geq \varepsilon_2 > 0$. This can occur in load situations with low shear stresses compared to the normal stresses and is recommended to be included only to ensure numerical stability since combining tension softening with tension stiffening can appear inconsistent. The exponential curve recommended by the Dutch guidelines for nonlinear finite element analyses (NLFEA) of concrete structures [3,29] is chosen for the tension softening of concrete, see Fig. 8(b). Here, $\varepsilon_{ctu} = G_f / \left[\max\left(S_{crx0}, S_{cry0}\right) f_{ct}\right]$ where it is for simplicity assumed that the fracture energy is smeared over the maximum crack spacing in either x or y direction.

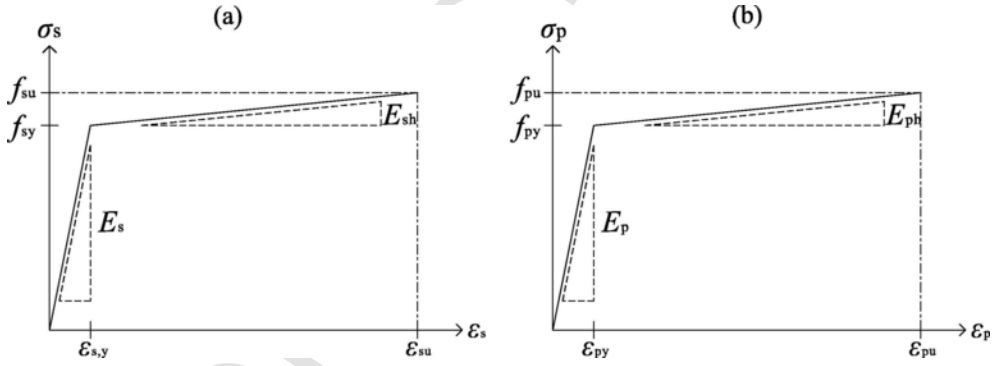

Fig. 7. (a) Bilinear behaviour of reinforcing steel bars. (b) Bilinear behaviour of prestressing steel.

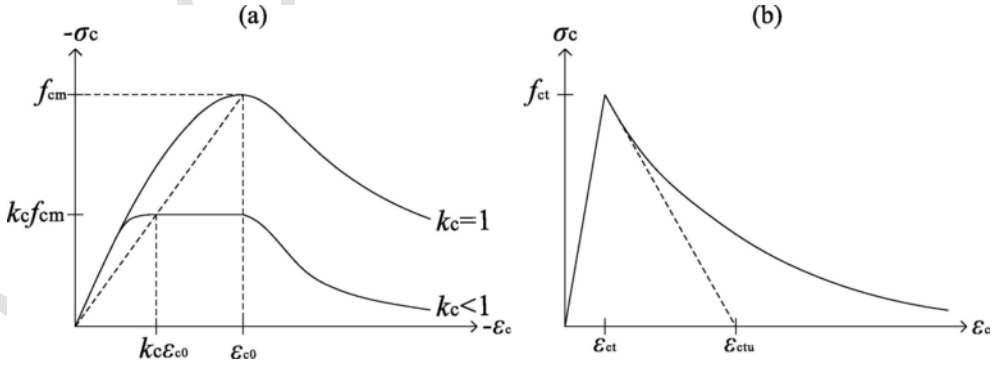

Fig. 8. (a) Compressive behaviour of concrete using the constitutive model of Foster and Marti [24]. (b) Tensile behaviour of concrete using the exponential curve recommended by the Dutch guidelines for NLFEA (Hendriks et al., 2017).

3.5. Constitutive relationships

The equilibrium in Eqs. (1)–(3) can be written as

$$\boldsymbol{\sigma}_{\mathrm{xy}} = \boldsymbol{D}_{\mathbf{xy}}\boldsymbol{\varepsilon}_{\mathbf{xy}} \tag{32}$$

in which the equilibrium in Eq. (32) is determined iteratively by updating the material elasticity tensor $\boldsymbol{D}_{\mathbf{xy}} = \boldsymbol{D}_{\mathbf{cxy}} + \boldsymbol{D}_{\mathbf{sxy}} + \boldsymbol{D}_{\mathbf{pxy}}$ using the secant stiffness. Here,

$$\boldsymbol{D}_{\mathbf{cxy}} = \boldsymbol{T}'\boldsymbol{D}_{\mathbf{c}12}\boldsymbol{T} \tag{33}$$

where $\boldsymbol{T}$ is the strain transformation tensor to the principal plane and

$$\boldsymbol{D}_{\mathbf{c}12} = \frac{1}{1-\nu_{c12}\nu_{c21}}\begin{bmatrix} E_{\mathrm{c1}} & \nu_{\mathrm{c12}}E_{\mathrm{c1}} & 0 \\ \nu_{\mathrm{c21}}E_{\mathrm{c2}} & E_{\mathrm{c2}} & 0 \\ 0 & 0 & \left(1-\nu_{\mathrm{c12}}\nu_{\mathrm{c21}}\right)G_{\mathrm{c12}} \end{bmatrix} \tag{34}$$

is the concrete elasticity tensor adopted from [13,24]. Here, ν_{c12} and ν_{c21} were the Poisson's ratio's taken as zero after cracking, and $\left(1-\nu_{\mathrm{c12}}\nu_{\mathrm{c21}}\right)G_{c12} = 1/4\left[E_{\mathrm{c1}}\left(1-\nu_{\mathrm{c12}}\right) + E_{\mathrm{c2}}\left(1-\nu_{\mathrm{c21}}\right)\right]$. The secant modules are determined from the chosen constitutive laws for concrete as $E_{\mathrm{c1}} = \sigma_{\mathrm{c1}}/\varepsilon_1$ and $E_{\mathrm{c2}} = \sigma_{\mathrm{c2}}/\varepsilon_2$. The elasticity tensors for reinforcing and prestressing steel are

$$\boldsymbol{D}_{\mathbf{sxy}} + \boldsymbol{D}_{\mathbf{pxy}} = \begin{bmatrix} \rho_{\mathrm{sx}}E_{\mathrm{sx}} & 0 & 0 \\ 0 & \rho_{\mathrm{sy}}E_{\mathrm{sy}} & 0 \\ 0 & 0 & 0 \end{bmatrix} + \begin{bmatrix} \rho_{\mathrm{px}}E_{\mathrm{px}} & 0 & 0 \\ 0 & \rho_{\mathrm{py}}E_{\mathrm{py}} & 0 \\ 0 & 0 & 0 \end{bmatrix} \tag{35}$$

in which the secant modules are determined as $E_{\mathrm{sx}} = \sigma_{\mathrm{srx}}/\varepsilon_{\mathrm{x}}$, $E_{\mathrm{sy}} = \sigma_{\mathrm{sry}}/\varepsilon_y$, $E_{\mathrm{px}} = \sigma_{\mathrm{prx}}/\varepsilon_{\mathrm{x}}$ and $E_{\mathrm{py}} = \sigma_{\mathrm{pry}}/\varepsilon_y$. Tension stiffening is neglected for the prestressing steel.

4. Simplified approach to calculate crack widths for RC membranes

The MCMM should provide more realistic estimates of the crack widths and deformations at a given load level. However, this would require some local iterations within the equilibrium iterations in the case of CHLM as discussed for Eq. (17), which *might* increase the calculation time. If the crack widths are of primary interest, a simplification to eliminate the local iterations would be to treat rebars as *unbonded*, i.e. using the constitutive law for naked reinforcing steel in Fig. 7a) instead of the MTCM to determine the equilibrium in Eq. (32). The tension stiffening is a posteriori accounted for by assuming that steel strains at the crack are $\varepsilon_{\mathrm{srx}} = \varepsilon_{\mathrm{x}}$ and $\varepsilon_{\mathrm{sry}} = \varepsilon_{\mathrm{y}}$ in determining $\lambda_{\mathbf{x}}$ and λ_{y} from Eqs. (21) and (22), after which the mean strains $\varepsilon_{\mathrm{smx}}$ and $\varepsilon_{\mathrm{smy}}$ are determined from the concept of either CLLM or CHLM to predict the crack width. This approach is analogous to predicting crack widths using the steel stresses at a cracked section, similar to as one would have done in a practical design situation for uniaxial stress conditions. The approach is conservative compared to using the MCMM.

5. Comparison with experimental results

5.1. General

Experimental results and predictions by the MCMM, the CMM using the TCM of Seelhofer [55] and the simplified approach are compared in the following. A similar comparison was conducted by [39]. The framework presented in Section 3 was used for the MCMM predictions, meaning that tension stiffening using the MTCM was accounted for in obtaining the equilibrium in Eq. (32) and thus the load-deformation response. Tension softening was excluded in the predictions of the MCMM, CMM and the simplified approach.

5.2. Predicted response of shear panels

The response predicted by the MCMM is now compared to a selection of experimental results of orthogonally RC panels available in the literature [63,36,43,65,40], see Table 1 for a summary of the material parameters. In summary, the selection consisted of panels with isotropic and anisotropic rebar layout, high strength concrete, prestressing and even unique loading conditions. The panels were loaded in pure shear except for PV25, which additionally was loaded in axial compression proportional to the shear stress level as $\sigma_{\mathrm{x}} = \sigma_{\mathrm{y}} = -0.69\tau_{\mathrm{xy}}$, and PV28, which additionally was loaded in axial tension proportional to the shear stress level as $\sigma_x = \sigma_y = 0.32\tau_{\mathrm{xy}}$. Furthermore, PP2 was prestressed in x-direction with prestressing steel ratio $\rho_{\mathrm{px}} = 0.29\%$, yield stress $f_{\mathrm{pyx}} = 910\mathrm{MPa}$, Young's modulus $E_{\mathrm{px}} = 200\mathrm{GPa}$ and an applied initial strain of $\varepsilon_{p0\mathrm{x}} = 3.53\%$■, while panel TA2 was prestressed in x-direction with prestressing steel ratio $\rho_{\mathrm{px}} = 0.84\%$, yield stress $f_{\mathrm{pyx}} = 1303\mathrm{MPa}$, Young's modulus $E_{\mathrm{px}} = 200\ \mathrm{GPa}$ and an applied initial strain of $\varepsilon_{p0\mathrm{x}} = 4.93\%$■. Note that TA2 was not reinforced with rebars in x-direction. The variety of panels selected for comparison was chosen mainly to investigate the ability of the MCMM to predict consistent load-deformation responses.

Comparison of experimental results and model predictions are shown in Fig. 9. As mentioned previously, the simplified approach does not include for tension stiffening in determining the equilibrium and yields thus larger deformations compared to the MCMM and CMM. It is also observed that there in general are small discrepancies between the MCMM and CMM, although the response after yielding of rebars looks to be slightly improved for the MCMM. Nevertheless, consistent and good predictions of the deformations and the ultimate load capacity are in general observed for both MCMM and CMM.

5.3. Crack widths

Comparison of crack widths predicted by the models are now compared to a selection of experimental results available in the literature at which the maximum crack widths measured were documented properly. The selection consisted of the test series by Tan et al. [57] on the RC ties X-20-40, X-32-40, X-20-90 and X-32-90, S and CS test series by

Table 1
Material parameters for selected RC panels.

Panel	Ref.	f_{cm} [MPa]	$\varepsilon_{\mathrm{c0}}$ [‰]	ϕ_{sx} [mm]	ρ_{sx} [%]	f_{syx} [MPa]	E_{sx} [MPa]	ϕ_{sy} [MPa]	ρ_{sy} [%]	f_{syy} [MPa]	E_{sy} [MPa]
PV25	Vecchio and Collins [63]	19.3	1.8	6.35	1.78	466	200	6.35	1.78	466	200
PV28		19	1.85	6.35	1.78	483	200	6.35	1.78	483	200
SE6	Khalifa [36]	40	2.5	19.5	2.93	492	200	11.3	0.32	479	200
PP2	Marti and Meyboom [43]	28.1	2.38	16	1.29	486	200	11.3	0.64	480	200
VA3	Zhang and Hsu [65]	94.6	2.45	19.5	3.41	455	200	19.5	3.41	455	200
TA2	Laskar et al. [40]	41.3	1.9	–	–	–	–	12.8	0.77	415	192

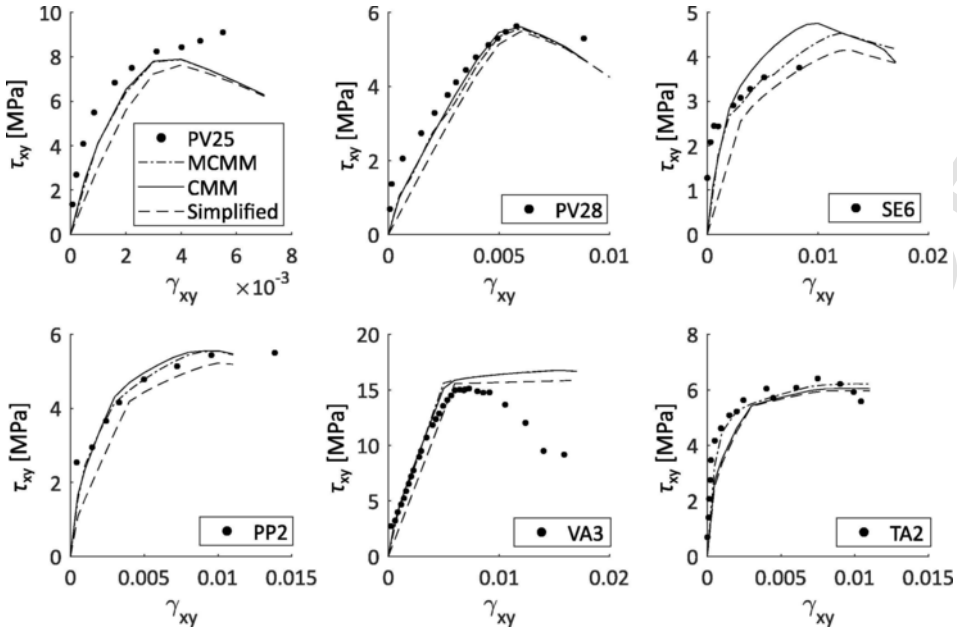

Fig. 9. Comparison between responses predicted by the MCMM, CMM and the simplified approach with experimental results.

Dyngeland [18], panel PP1 by Marti and Meyboom [43], A and B test series by Pang [49] and KS test series by Proestos [52]. A summary including loading, reinforcement layout, maximum crack widths measured experimentally $w_{\max}$ and crack widths predicted w_{cr} is given in Table 2. Further details regarding material properties, mechanical properties and test setup were else fully provided in the respective references. The axially loaded RC ties were included mainly to investigate how well the MCMM and the CMM captures the effects of large rebars and covers. Moreover, it is noticed that the S and CS panels were axially loaded only, however, with varying inclination for the orthogonal rebar grid in which α_s denotes the angle counter clockwise between the longitudinal reinforcement and the global x-direction. This was conveniently accounted for in the calculations by obtaining steel stresses at the crack in terms of the mean strains in the α_s-direction for the tension stiffening of the longitudinal reinforcement and the mean strains normal to the α_s -direction for the tension stiffening of the transversal reinforcement.

Fig. 10(a) shows comparison of mean and maximum crack widths measured experimentally and crack widths predicted by the models for six of the panels in Table 2. Corresponding load deformations responses are also included in Fig. 10(b). It is in general observed good agreement between maximum crack widths measured and crack widths predicted as well as between load deformation responses. The exception is CS2, at which the models yield quite conservative predictions. This can be explained by the fact that transversal pressure was applied normal to the loading direction, which would have beneficial effect on the tension stiffening as discussed by Dyngeland [18]. Similar was observed in the experiments by Dörr [17] at which it was seen that the tension stiffening enchanced with increasing confining pressure for uniaxially loaded specimens. This beneficial effect is not captured by the MCMM nor the CMM since the bond-slip curves adopted were based on the behaviour of uniaxial loaded RC ties in tension. Similar trend was observed for PV25. Furthermore, the discontinuity observed for the MCMM and the simplified approach is caused by the transition between the CLLM and CHLM.

5.4. The modelling uncertainty for crack width predictions

The modelling uncertainty for crack widths predicted, i.e.

$$\theta = \frac{w_{\max}}{w_{cr}} \tag{36}$$

was investigated for the MCMM, CMM and the simplified approach. The statistical properties of θ were obtained using the method of Engen et al. [23] and Tan et al. [57], which implied assuming log-normal distribution for the modelling uncertainty in accordance with the recommendations in JCSS Probabilistic Model Code [33] This means that the natural logarithm of θ is assumed normal distributed. Values for θ are shown in Table 2, presented graphically in Fig. 11 and summarized in Table 3 showing the statistical properties for the modelling uncertainty such as mean, variance, standard deviation *SD*, coefficient of variation *COV* , minimum and maximum values for θ and the number of observations $n(\theta > 1)$ at which the crack widths measured exceed the crack widths predicted. A total of 101 observations for θ were obtained from Table 2. The summary suggests that the MCMM and the simplified approach show greater potential for predicting crack widths than the CMM.

6. Discussion

The results show that the simplified approach provided most conservative predictions, as expected. This can be explained by the fact that the simplified approach predicts crack widths using shear strains γ_{xy} when tension stiffening is neglected. Furthermore, it is observed that the CMM yielded a mean value for the modelling uncertainty on the nonconservative side while being more inconsistent in its predictions than the MCMM and the simplified approach which is reflected by the observations that it has the largest SD and COV. Table 2 shows that the CMM in particular underestimated the crack widths considerably for RC ties with the combination of large rebar and cover, e.g. X-32-90. The MCMM, on the other hand, provided a mean closest to one on the conservative side and yielded more consistent predictions in comparison which can be observed by the fact that it exhibits the lowest COV. This statement can also be backed up from a mechanical point

Table 2
Crack widths for investigated specimen.

Dimension	Panel	τ_{xy}	σ_x	σ_y	α_s	Cover	ϕ_{sx}	ϕ_{sy}	ρ_{sx}	ρ_{sy}	w_{max}	$w_{cr,MCMM}$	$w_{cr,CMM}$	$w_{cr,simp}$	θ_{MCMM}	θ_{CMM}	θ_{simp}
[mm]		[MPa]			[deg]	[mm]	[mm]		[%]		[mm]						
3000 × 400 × 400	X-20-40	–	3.14	–	0	40	20.00	–	1.57	–	0.13	0.24	0.11	0.24	0.55	1.25	0.55
		–	3.25	–							0.13	0.26	0.12	0.26	0.52	1.14	0.52
		–	4.17	–							0.16	0.37	0.19	0.37	0.44	0.85	0.44
		–	5.05	–							0.22	0.42	0.28	0.42	0.51	0.78	0.51
	X-32-40	–	4.71	–	0	40	32.00	–	4.02	–	0.08	0.15	0.05	0.15	0.55	1.58	0.55
		–	4.64	–							0.07	0.14	0.05	0.14	0.47	1.38	0.47
		–	6.33	–							0.10	0.18	0.09	0.18	0.53	1.09	0.53
	X-20-90	–	3.66	–	0	90	20.00	–	1.57	–	0.21	0.30	0.15	0.30	0.68	1.42	0.68
		–	3.59	–							0.21	0.30	0.14	0.30	0.72	1.51	0.72
		–	4.60	–							0.31	0.43	0.23	0.43	0.72	1.33	0.72
		–	6.27	–							0.40	0.56	0.40	0.56	0.72	1.01	0.72
	X-32-90	–	5.03	–	0	90	32.00	–	4.02	–	0.16	0.16	0.06	0.16	0.99	2.76	0.99
		–	5.03	–							0.17	0.16	0.06	0.16	1.04	2.91	1.04
		–	6.28	–							0.21	0.18	0.09	0.18	1.16	2.42	1.16
		–	7.51	–							0.24	0.23	0.12	0.23	1.05	2.05	1.05
		–	8.52	–							0.27	0.27	0.14	0.27	1.00	1.89	1.00
630 × 630 × 100	S1	–	3.76	–	0	10	8.00	8.00	1.12	–	0.15	0.21	0.18	0.21	0.72	0.84	0.72
	S2	–	3.56	–	0				1.12	–	0.14	0.19	0.16	0.19	0.72	0.86	0.72
	S3	–	3.80	–	45.00				1.12	1.12	0.29	0.33	0.40	0.40	0.87	0.72	0.72
	S4	–	3.49	–	45.00				1.12	1.12	0.30	0.30	0.35	0.37	1.00	0.85	0.82
	S5	–	2.67	–	45.00				0.56	1.12	0.41	0.83	0.45	1.74	0.49	0.90	0.23
	S6	–	3.41	–	18.40				1.12	1.12	0.17	0.27	0.19	0.35	0.64	0.90	0.49
	S7	–	3.45	–	18.40				1.12	0.37	0.32	0.81	0.49	1.04	0.40	0.65	0.31
	S8	–	3.41	–	18.40				1.12	1.12	0.16	0.27	0.19	0.35	0.60	0.84	0.46
	CS1	–	3.74	−4.67	0				1.12	–	0.08	0.20	0.21	0.20	0.40	0.38	0.40
	CS2	–	3.74	−9.34	0				1.12	–	0.08	0.20	0.21	0.20	0.40	0.38	0.40
	CS3	–	3.74	−4.67	45.00				1.12	1.12	0.30	0.34	0.35	0.39	0.89	0.86	0.76
	CS4	–	3.74	−9.34	45.00				1.12	1.12	0.42	0.36	0.37	0.41	1.17	1.14	1.01
	CS6	–	3.74	–	0				1.12	1.12	0.14	0.20	0.21	0.20	0.69	0.66	0.69
1626 × 1626 × 287	PP1	1.72	–	–	0	22	19.50	11.30	1.94	0.65	0.16	0.23	0.18	0.45	1.35	1.23	0.68
		2.15	–	–							0.20	0.34	0.26	0.41	1.39	1.05	1.19
		2.64	–	–							0.25	0.44	0.37	0.54	0.77	0.65	0.79
		3.04	–	–							0.29	0.53	0.46	0.63	0.76	1.21	0.49
		3.71	–	–							0.42	0.67	0.61	0.79	1.05	1.10	0.88
		4.14	–	–							0.58	0.89	0.72	1.09	0.62	0.59	0.54
1400 × 1400 × 178	A2	1.58	–	–	0	22	16.00	16.00	1.19	1.19	0.24	0.18	0.20	0.36	1.25	1.33	1.21
		2.78	–	–							0.50	0.36	0.47	0.42	0.56	0.67	0.51
		4.06	–	–							0.50	0.65	0.77	0.63	0.55	0.71	0.53
	A3	1.46	–	–	0	19	19.50	19.50	1.77	1.77	0.10	0.13	0.08	0.20	0.74	0.94	0.72
		2.76	–	–							0.25	0.24	0.23	0.29	0.67	0.84	0.65
		4.30	–	–							0.25	0.41	0.42	0.46	0.43	0.39	0.33
		7.06	–	–							1.02	0.81	0.77	0.84	0.42	0.38	0.37
	A4	4.69	–	–	0	13	25.20	25.20	2.95	2.95	0.16	0.28	0.24	0.31	0.53	0.46	0.45
		6.55	–	–							0.25	0.46	0.35	0.48	0.76	0.71	0.63
		8.69	–	–							0.46	0.62	0.49	0.64	1.26	1.16	0.97
		10.55	–	–							0.51	0.76	0.60	0.78	0.96	1.49	0.63
	B1	1.82	–	–	0	22	16.00	11.30	1.19	0.59	0.15	0.34	0.38	0.44	0.34	0.36	0.30
		2.28	–	–							0.21	0.50	0.55	0.57	0.23	0.24	0.21
		2.71	–	–							0.33	0.62	0.72	0.73	1.48	1.49	1.33
		3.23	–	–							0.66	0.87	0.94	1.05	1.69	1.80	1.38
		3.71	–	–							1.66	1.32	1.43	1.70	1.22	1.12	1.05
	B2	1.68	–	–	0	19	19.50	16.00	1.77	1.19	0.21	0.22	0.14	0.33	1.65	2.07	0.99
		3.86	–	–							0.18	0.52	0.50	0.59	1.57	1.71	1.36

Table 2 (*Continued*)

Dimension	Panel	τ_{xy}	σ_x	σ_y	α_s	Cover	ϕ_{sx}	ϕ_{sy}	ρ_{sx}	ρ_{sy}	w_{max}	$w_{cr,MCMM}$	$w_{cr,CMM}$	$w_{cr,simp}$	θ_{MCMM}	θ_{CMM}	θ_{simp}
[mm]		[MPa]			[deg]	[mm]	[mm]		[%]		[mm]						
	B3	1.89	–	–	0	19	19.50	11.30	1.77	0.59	0.57	0.34	0.32	0.41	0.72	0.86	0.65
		3.12	–	–							0.75	0.62	0.67	0.72	0.56	0.65	0.51
	B4	1.58	–	–	0	13	25.20	11.30	2.95	0.59	0.37	0.22	0.18	0.37	0.76	0.97	0.77
		2.96	–	–							0.77	0.49	0.45	0.56	1.14	1.44	1.09
	B5	2.54	–	–	0	13	25.20	16.00	2.95	1.19	0.24	0.27	0.20	0.30	1.28	1.65	0.66
		3.75	–	–							0.32	0.42	0.35	0.48	1.11	1.31	0.94
		4.31	–	–							0.36	0.49	0.41	0.55	0.66	0.83	0.64
		5.46	–	–							0.36	0.65	0.56	0.71	0.72	0.91	0.37
		6.13	–	–							0.62	0.81	0.64	0.81	0.59	0.78	0.50
		6.55	–	–							0.99	0.87	0.69	0.91	0.55	0.67	0.46
	B6	2.17	–	–	0	13	25.20	19.50	2.95	1.77	0.20	0.16	0.12	0.30	0.55	0.64	0.47
		2.97	–	–							0.25	0.23	0.19	0.27	0.62	0.68	0.53
		6.14	–	–							0.40	0.60	0.48	0.63	0.66	0.81	0.53
1626 × 1626 × 355	KS1	2	–	–	0	54	16	12.8	2.09	1.35	0.20	0.18	0.08	0.29	1.11	2.37	0.69
		4	–	–							0.35	0.36	0.27	0.44	0.97	1.31	0.80
		6	–	–							1.10	0.63	0.46	0.71	1.74	2.37	1.54
	KS2	2	0.8	0.8	0	54	16	12.8	2.09	1.35	0.10	0.28	0.14	0.47	0.35	0.70	0.21
		3	1.2	1.2							0.30	0.37	0.28	0.45	0.81	1.09	0.66
		4	1.6	1.6							0.65	0.57	0.41	0.65	1.15	1.59	1.01
	KS3	3	−1.2	−1.2	0	54	16	12.8	2.09	1.35	0.15	0.17	0.08	0.26	0.87	1.84	0.57
		6	−2.4	−2.4							0.35	0.34	0.25	0.42	1.02	1.40	0.84
		9	−3.6	−3.6							0.65	0.61	0.45	0.69	1.06	1.46	0.94
	KS4	2	–	–	0	54	16	16	1.57	1.04	0.20	0.30	0.16	0.50	0.67	1.29	0.40
		4	–	–							0.60	0.67	0.49	0.79	0.90	1.21	0.76
		6	–	–							1.10	1.07	0.86	1.22	1.02	1.27	0.90
	KS5	2	0.8	0.8	0	54	16	16	1.57	1.04	0.15	0.47	0.25	0.81	0.32	0.59	0.19
		3	1.2	1.2							0.55	0.70	0.49	0.84	0.78	1.11	0.65
		4	1.6	1.6							1.10	0.99	0.74	1.15	1.11	1.48	0.96
	KS6	2	−0.8	−0.8	0	54	16	16	1.57	1.04	0.15	0.15	0.07	0.24	0.99	2.12	0.62
		5	−2	−2							0.50	0.44	0.32	0.58	1.12	1.58	0.86
		7	−2.8	−2.8							0.75	0.77	0.54	0.90	0.98	1.38	0.84
		9	−3.6	−3.6							1.30	1.04	0.78	1.19	1.25	1.66	1.09
	KS7	2	–	–	0	54	16	12.8	2.09	1.35	0.20	0.18	0.08	0.29	1.12	2.54	0.69
		5	–	–							0.65	0.52	0.35	0.60	1.24	1.85	1.08
		7	–	–							0.80	0.78	0.55	0.87	1.03	1.46	0.92
		9	–	–							1.20	1.14	0.75	1.20	1.05	1.59	1.00
	KS8	2	0.8	0.8	0	54	16	12.8	2.09	1.35	0.10	0.28	0.13	0.47	0.36	0.75	0.22
		3	1.2	1.2							0.50	0.38	0.26	0.47	1.33	1.90	1.07
		5	2	2							0.90	0.75	0.53	0.85	1.20	1.70	1.06
	KS9	2	–	–	0	54	16	16	1.57	1.04	0.15	0.29	0.11	0.49	0.52	1.31	0.30
		4	–	–							0.60	0.63	0.39	1.38	0.95	1.55	0.43
		6	–	–							1.10	1.19	0.74	1.40	0.93	1.49	0.78
	KS10	2	−0.6	−0.6	0	54	16	16	1.57	1.04	0.40	0.18	0.07	0.30	2.23	5.75	1.35
		5	−1.5	−1.5							0.60	0.55	0.32	1.16	1.09	1.88	0.52
		8	−2.4	−2.4							1.00	1.13	0.70	1.33	0.88	1.44	0.75
		9	−2.7	−2.7							1.50	1.30	0.83	1.51	1.15	1.82	0.99

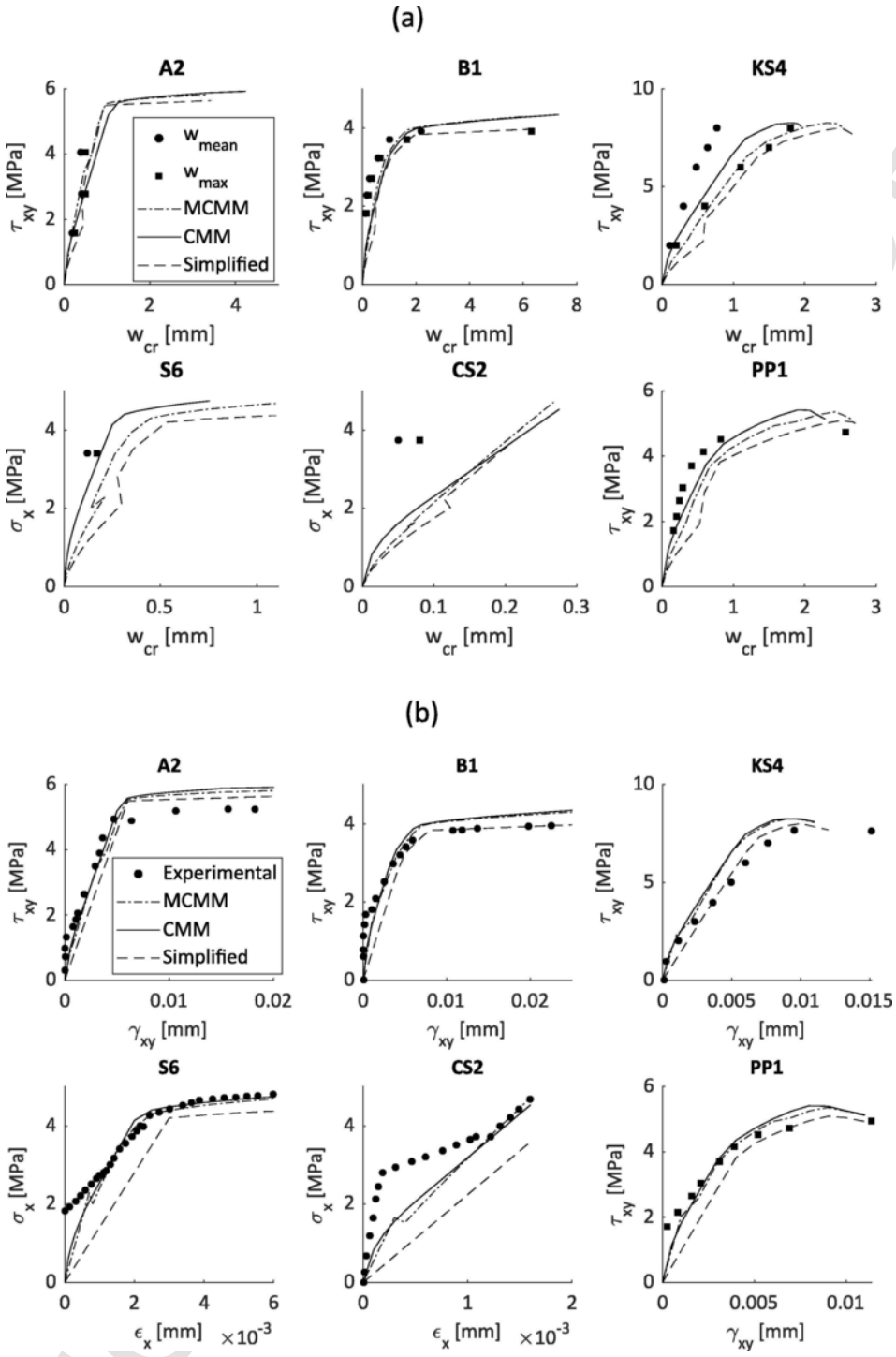

Fig. 10. (a) Comparison between mean and maximum crack widths measured experimentally and crack widths predicted by the MCMM, CMM and the simplified approach. (b) Comparison between corresponding load deformation responses predicted by the MCMM, CMM and the simplified approach with experimental results.

of view since the MCMM accounts for all cracking stages through the concepts of CLLM and CHLM behaviour, whereas the CMM in principle applies to the stabilized cracking stage only. Also, solving the SODE for the slip using the MC2010 bond-slip law in the MTCM is a mechanical improvement to the TCM, and should better account for the effects of large rebars and covers as well as rebar spacing, thus offering wider range of applicability as discussed by Tan et al. [60].

It is noticed from Table 3 that the *COV* is relatively large in comparison with the *COV* for the modelling uncertainty of the ultimate load capacity reported in e.g. [5,51]. Relatively large *COV* for the modelling uncertainty of crack widths predicted have also been reported in recent studies [21,57,22]. This is first and foremost owing to the large scatter in tensile strength of concrete and its influence on generating a random crack pattern as discussed by Barre et al. [2] and Tan et al. [58]. Secondly, the modelling uncertainty for predicting the maximum crack widths becomes sensitive to the many physical uncertainties related to the chosen measuring technique. Most simply measure the maximum crack widths by the eye, others use more refined measuring techniques such as image analysis or digital image correlation while

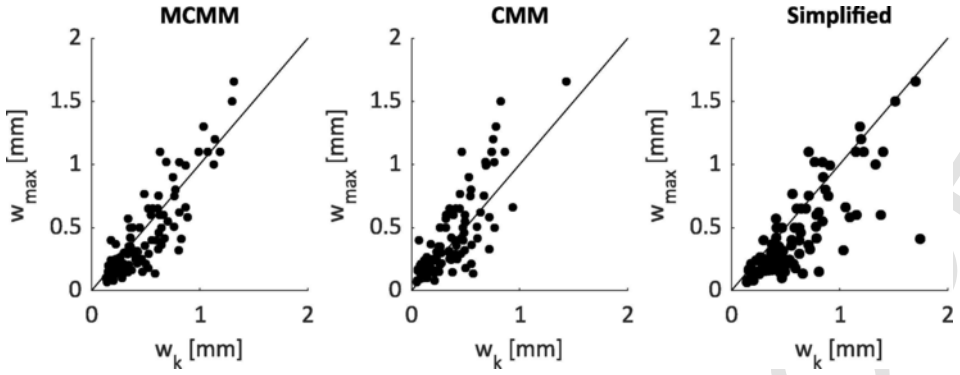

Fig. 11. Maximum crack widths measured experimentally versus crack widths predicted by the MCMM, CMM and the simplified approach for the 101 observations for the modelling uncertainty.

Table 3
Modelling uncertainty for crack width predictions.

Model	Mean	Variance	*SD*	*COV*	Min	Max	$n(\theta>1)$
MCMM	0.88	0.19	0.40	0.45	0.23	2.23	36
CMM	1.28	0.27	0.72	0.56	0.24	5.75	61
Simplified	0.73	0.21	0.35	0.48	0.19	1.54	19

some use statistics to determine the 95%-quantile of the maximum crack widths measured. Another important physical aspect is related to where the maximum crack widths measured apply at the specimen surface, since they in general vary significantly depending on if they are measured over the rebar or between two adjacent rebars as discussed by Dawood and Marzouk [14], not to mention the uncertainties related to the calculation model itself [42,45].

All three models can be extended to predict the cracking behaviour of RC shell sections, e.g. by implementation to a layered approach. The authors of this paper are currently working on such an approach. It is also recommended to conduct further probabilistic analysis on the modelling uncertainty for crack width predictions to better understand the main parameters influencing the cracking behaviour. Such studies can be important in developing crack width calculation models in general.

7. Conclusions

The modified cracked membrane model (MCMM) presented in this paper was formulated to facilitate a mechanical calculation model that is able to predict crack widths in orthogonally reinforced concrete (RC) membranes subjected to in-plane loading. It was formulated using the basic concepts of the cracked membrane model (CMM), the essential difference being a replacement of the tension chord model (TCM) with the modified tension chord model (MTCM). A generalized expression to determine the tension stiffening normal to the crack in RC membranes was formulated, a feature currently missing in Eurocode 2 and *fib* Model Code 2010. Also, a simplified approach for predicting crack widths in RC membranes was proposed. The crack widths predicted by the MCMM, the cracked membrane model (CMM) and the simplified approach were compared to a total of 101 maximum crack widths measured experimentally on 37 test specimens to discover the modelling uncertainty. The CMM showed a mean value for the modelling uncertainty on the nonconservative side and yielded more inconsistent crack width predictions in particular for the combination of large rebars and covers. The MCMM, on the other hand, provided a mean closest to one on the conservative side and was observed to be more consistent in terms of having the lowest coefficient of variation in comparison with the CMM, which could be attributed to its mechanical improvement, hence, offering a wider range of applicability. The simplified approach yielded in average most conservative predictions as expected. Finally, the results in this paper suggests that both the MCMM and the simplified approach show great potential for yielding reliable crack width predictions in RC membranes, whereas the MCMM showed good predictions of deformations and ultimate capacity as well.

Acknowledgement

The work presented in this paper is part of an ongoing PhD study funded by the Norwegian Public Roads Administration as a part of the Coastal Highway Route E39 project.

References

[1] G.L. Bálasz, Cracking analysis based on slip and bond stresses, ACI Mater J 90 (4) (1993) 340–348.
[2] F. Barre, P. Bisch, D. Chauvel, et al., Control of cracking in reinforced concrete structures: research project CEOS.fr (Civil Engineering and Geomechanics), ISTE Ltd, London, UK, 2016.
[3] B. Belletti, C. Damoni, M.A.N. Hendriks, A. de Boer, "Analytical and numerical evaluation of the design resistance of reinforced concrete slabs", fib J Struct Concr 15 (3) (2014) 1436–1447.
[4] E.C. Bentz. Sectional analysis of reinforced concrete members. PhD-thesis, Department of Civil Engineering, University of Toronto, Toronto, Canada; 2000.
[5] E.C. Bentz, F.J. Vecchio, M.P. Collins, Simplified modified compression field theory for calculating shear strength of reinforced concrete elements, ACI Struct J 103 (4) (2006) 614–624.
[6] L.F.A. Bernardo, A.R.B. Lyrio, J.R.B. Silva, B. Horowitz, Refined softened truss model with efficient solution procedure for prestressed concrete membranes, J Struct Eng 144 (6) (2018) https://doi.org/10.1061/(ASCE)ST.1943-541X.0002044.
[7] B. Borosnyói, G.L. Balázs, Crack width variation within the concrete cover of reinforced concrete members, fib J Struct Concr 62 (3) (2005) 53–62.
[8] CEN. EN 1992-1-1 Eurocode 2: Design of Concrete Structures – Part 1-1: General Rules and Rules for buildings. Brussels, Belgium: European Committee for Standardization; 2004.
[9] R. Cerioni, I. Iori, P. Michelini, P. Bernardi, Multi-directional modeling of crack pattern in 2D R/C members, Eng Fract Mech 75 (3–4) (2007) 615–628.
[10] Collins MP, Porasz A. Shear strength for high strength concrete. Bulletin No. 193, Design Aspects of High Strength Concrete. Comité Euro-International du Béton; 1989. p. 75–83.
[11] M.P. Collins, D. Mitchell, Prestressed concrete structures, Prentice Hall Inc, New Jersey, USA, 1997.
[12] H. Dabbagh, S.J. Foster, A smeared – fixed crack model for FE analysis of RC membranes incorporating aggregate interlock, Adv Struct Eng 9 (1) (2006) 91–101.
[13] D. Darwin, D.A. Pecknold, Nonlinear biaxial stress-strain law for concrete, J Eng Mech Div, ASCE 103 (2) (1977) 229–241.
[14] N. Dawood, H. Marzouk, Crack width model for thick reinforced concrete plates subjected to in-plane forces, Can J Civ Eng 38 (11) (2011) 1262–1273.
[15] P.G. Debernardi, M. Taliano, An improvement to Eurocode 2 and fib Model Code 2010 methods for calculating crack width in RC structures, fib J Struct Concr 17 (3) (2016) 365–376.
[16] DIN: EN 1992-1-1/NA. 2011-01, National Annex – Nationally determined parameters – Eurocode 2: Design of concrete structures – Part 1-1: General rules and rules for buildings; 2011.
[17] Dörr K. Bond-behaviour of ribbed reinforcement under transversal pressure. In: IASS symposium on nonlinear behaviour of reinforced concrete spatial structures. Werner Verlag, Düsseldorf, Germany, Vol. 1; 1978. p. 13–24.
[18] Dyngeland T. Behaviour of reinforced concrete panels. PhD-thesis, Department of Structural Engineering. Trondheim, Norway: Norwegian University of Science and Technology; 1989.
[19] A.D. Edwards, A. Picard, Theory of cracking in concrete members, Proc ASCE – J Struct Div 98 (12) (1972) 2687–2700.

[20] R. Eligehausen, E.P. Popov, V.V. Bertero, Local bond stress-slip relationships of deformed bars under generalized excitations". Report No. UCB/EERC 83–23, University of California, Berkeley, USA, 1983.
[21] Empelmann M, Sawicki P, Busse D. Comparison of analysis concepts for crack width limitation in accordance with EN 1992-1-1, DIN EN 1992-1-1/NA as well as Model Code 2010. Report Nr. P02-19-1A. iBMB, TU Braunschweig, Germany; 2016.
[22] Empelmann M, Busse D. Prediction accuracy of code provisions for the calculation of crack widths. In: fib Congress, October 2018, Melbourne, Australia; 2018, ISBN 978-1-877040-14-6.
[23] M. Engen, M.A.N. Hendriks, J. Köhler, et al., A quantification of the modelling uncertainty of non-linear finite element analyses of large concrete structures, Struct Saf 64 (1) (2017) 1–8.
[24] S.J. Foster, P. Marti, Cracked membrane model: finite element implementation, J Struct Eng 129 (9) (2003) 1155–1163.
[25] fib. Structural Concrete. Textbook on behaviour, design and performance. Second edition. Volume 2. fib bulletin No. 52, Lausanne, Switzerland; 2010.
[26] fib. fib Model Code for Concrete Structures 2010. International Federation for Structural Concrete." Ernst & Sohn, Berlin; 2013.
[27] L. Giordano, G. Mancini, Crack width evaluation of reinforced concrete membrane elements, Struct Eng Int 19 (3) (2009) 256–261.
[28] Y. Goto, Crack formed in concrete around deformed tension bars, ACI J 68 (4) (1971) 244–251.
[29] M.A.N. Hendriks, A. de Boer, B. Belletti, Guidelines for nonlinear finite element analysis of concrete structures (RTD: 1016–1: 2017), Rijkswaterstaat Centre for Infrastructure, Utrecht, the Netherlands, 2017.
[30] T.T.C. Hsu, Softened truss model theory for shear and torsion, ACI Struct J 85 (6) (1988) 624–635.
[31] T.T.C. Hsu, Y.L. Mo, Unified theory of concrete structures, Wiley, Chichester, UK, 2010.
[32] F. Irgens, Continuum mechanics, Springer, Bergen, Norway, 2008.
[33] JCSS. Probabilistic model code, 12th draft." Joint Committee on Structural Safety; 2001.
[34] D.H. Jiang, S.P. Shah, A.T. Andonian, Study of the transfer of tensile forces by bond, ACI J 81 (4) (1984) 251–259.
[35] S. Khalfallah, Cracking analysis of reinforced concrete tensioned members, fib J Struct Concr 7 (3) (2006) 111–116.
[36] J. Khalifa, Limit analysis and design of reinforced concrete shell elements, PhD-thesis Department of Civil Engineering, University of Toronto, Toronto, Canada, 1986.
[37] W. Kaufmann, Strength and deformations of structural concrete subjected to in-plane shear and normal forces, PhD-thesis Institute of Structural Engineering, Swiss Federal Institute of Technology, Zürich, Switzerland, 1998.
[38] W. Kaufmann, P. Marti, Structural concrete: cracked membrane model, J Struct Eng 124 (12) (1998) 1467–1475.
[39] Kaufmann W, Mata-Falcón J. Crack widths in structural concrete subjected to in-plane loading. In: Workshop proceedings No. 12 on Crack width calculation methods for large concrete structres, Nordic Concrete Federation, Norsk Betongforening, Oslo, Norway; 2017.
[40] Laskar A, Wang J, Hsu TTC, Mo YL. Rational shear provisions for AASHTO LRFD specifications: TECHNICAL REPORT. Report No. FHWA/TX-07/0-4759-1. In: Department of Civil & Environmental Engineering, Cullen College of Engineering, University of Houston, Houston, Texas, USA; 2007.
[41] L.A. Lutz, Analysis of stresses in concrete near a reinforcing bar due to bond and transverse cracking, ACI J 67 (10) (1970) 778–787.
[42] Markova J, Sykora M. Uncertainties in crack width verification of reinforced concrete structures. Risk, Reliab Saf: Innovating Theory Practice 2016, https://doi.org/10.1201/9781315374987-368.
[43] P. Marti, J. Meyboom, Response of prestressed concrete elements to in-plane shear forces, ACI Struct J 89 (5) (1992) 503–514.
[44] P. Marti, M. Alvarez, W. Kaufmann, V. Sigrist, Tension chord model for structural concrete, Struct Eng Int 8 (4) (1998) 287–298.
[45] M. Mlcoch, M. Markova, M. Sykora, Uncertainty in crack width estimates according to fib Model Code 2010, Civ Eng Series 17 (1) (2017) 155–158.
[46] S.M. Mirza, J. Houde, Study of bond stress-slip relationships in reinforced concrete, ACI J 76 (1) (1979) 19–46.
[47] A.H. Nilson, Internal measurement of bond slip, ACI J 69 (7) (1972) 439–441.
[48] NPRA. N400 Bruprosjektering: Prosjektering av bruer, ferjekaier og andre bærende konstruksjoner. N400 i Statens vegvesens håndbokserie; 2015, ISBN: 978-82-7207-680-0.
[49] X.B. Pang, Constitutive laws of Reinforced Concrete in Shear, PhD-thesis Department of Civil and Environmental Engineering, University of Houston, Houston, USA, 1991.
[50] X.B. Pang, T.T.C. Hsu, Behavior of reinforced concrete membrane elements in shear, ACI Struct J 92 (6) (1995) 665–679.
[51] M. Pimentel, E. Brüwhiler, J. Figueiras, Extended cracked membrane model for the analysis of RC panels, Eng Struct 32 (8) (2010) 1964–1975.
[52] G.T. Proestos, Influence of high-strength reinforcing bars on the behaviour of reinforced concrete nuclear containment structures subjected to shear, M. Sc-thesis Department of Civil Engineering, University of Toronto, Toronto, Canada, 2014.
[53] G. Russo, F. Romano, Cracking response of RC members subjected to uniaxial tension, J Struct Eng 118 (5) (1992) 1172–1190.
[54] Saliger R. High-grade steel in reinforced concrete. In: Proceedings of the 2nd Congress of the International Association for Bridge and Structural Engineering, Berlin-Munich, Germany. ETH Zürich, Switzerland; 1936. p. 293–15.
[55] Seelhofer H. Ebener Spannungszustand im Betonbau Grundlagen und Anwendungen. PhD-thesis, Zürich, Switzerland: Institute of Structural Engineering, Swiss Federal Institute of Technology; 2009.
[56] S. Somayaji, S.P. Shah, Bond stress versus slip relationship and cracking response of tension members, ACI J 78 (3) (1981) 217–225.
[57] R. Tan, K. Eileraas, O. Opkvitne, et al., Experimental and theoretical investigation of crack width calculation methods for RC ties, fib J Struct Concr 19 (5) (2018) 1436–1447.
[58] Tan R, Hendriks MAN, Geiker M, Kanstad T. A numerical investigation of the cracking behaviour of reinforced concrete tie elements. In: Magazine of Concrete Research, 2018b Ahead of Print, DOI: 10.1680/jmacr.18.00156.
[59] Tan R, Hendriks MAN, Kanstad T. An investigation of the strain profile over the cover in reinforced concrete elements subjected to tension. In: Proceedings for the 5th fib Congress, October 2018, Melbourne, Australia; 2018c. ISBN 978-1-877040-14-6.
[60] Tan R, Hendriks MAN, Geiker M, Kanstad T. Analytical calculation model for predicting the cracking behavior of reinforced concrete. ASCE J Struct Eng 2019 [in press].
[61] K. Tammo, K. Lundgren, S. Thelandersson, Nonlinear analysis of crack widths in reinforced concrete, Mag Concr Res 61 (1) (2009) 23–34.
[62] Thorenfeldt E, Tomaszewicz A, Jensen JJ. Mechanical properties of high-strength concrete and applications in design. In: Proceedings International Symposium on Utilization of High-Strength Concrete, Stavanger, Norway; 1987. p. 149–59.
[63] F.J. Vecchio, M.P. Collins, The response of reinforced concrete to in-plane shear and normal stresses, Department of Civil Engineering, University of Toronto, Toronto, Canada, 1982.
[64] F.J. Vecchio, M.P. Collins, The modified compression-field theory for reinforced concrete elements subjected to shear, ACI Struct J 83 (2) (1986) 219–231.
[65] L.X. Zhang, T.T.C. Hsu, Behavior and analysis of 100 MPa concrete membrane elements, J Struct Eng 124 (1) (1998) 24–34.